Single-Crystalline Gold Microplates: Synthesis, Characterization, and Thermal Stability

Caixia Kan,*,† Xiaoguang Zhu,‡ and Guanghou Wang†

National Laboratory of Solid State Microstructures and Department of Physics, Nanjing University, Nanjing, 210093, P. R. China, Institute of Solid State Physics, Chinese Academy of Sciences, Hefei, 230031, P. R. China

Received: August 25, 2005

Single-crystalline gold microplates of several 10 μm in lateral size, characterized by hexagonal, truncated triangular, and triangular shapes with (111) planes as two basal surfaces, have been synthesized in large quantities through a solution phase process. Significantly, such anisotropic Au nanostructures exhibit remarkable optical properties, in which the dipole plasmon resonance shifting in the NIR region and the quadrupole plasmon resonance at ∼820 nm were observed. Fragmentation of Au microplates is found when the temperature is higher than 450 °C, indicating they are not thermodynamically stable structure at high temperature. Investigations on the Au microplates upon heating suggest that the melting and collapsing start mainly at the edges that should be Au (110) facets. This work is valuable for Au nanostructures applied at elevated temperatures.

1. Introduction

Noble metal nanoparticles show significance of not only new or improved catalytic and electronic properties, but also distinctive shape-dependent optical properties that attracted great technological interest. This is particularly true for gold and silver nanostructures. Under certain conditions of morphological anisotropy, they exhibit anisotropic optical absorption properties associated with the collective oscillations of conduction electrons (known as surface plasmon resonance or SPR).[1] For Au (or Ag) nanospheres, a single SPR band is expected. However, more than one single resonance can be excited in a nonspherical nanostructure, irrespective of its size. For Ag nanowires with a triangular section, for instance, several resonances are expected for each illumination direction.[2] Experimentally, Au and Ag nanoparticles with a variety of shapes and dimensions are readily available through physical or chemical approaches. This includes one-dimensional nanorods or nanowires,[3] two-dimensional (2-D) nanodisks or polygonal nanostructures,[4] and three-dimensional polyhedron, nanocages or nanopods.[5]

Among these anisotropic nanostructures, 2-D nanoparticles with regular shapes (such as triangular), in particular, have generated intense interest in recent years due to their attractive optical properties. For example, Ag nanodisks display an in-plane dipole plasmon absorption peak that can be red shifted up to 1000 nm in the near-infrared (NIR) region.[6] Such an absorption extension opens new possibilities for biomedical diagnostics and other related fields.[7] For the interests of science and technology, solution-phase methods either thermally or photochemically have been recently established to synthesize Ag nanoprisms and nanodisks with precise size control, and their plasma resonances have been identified and assigned through experiment and computation.[4] In contrast to a large amount of reports on the two-dimensional planar Ag nanostructures, the synthesis of anisotropic Au nanoparticles is mainly limited (at least in high yield) to nanorods, and planar Au nanostructures are less well-known, although a few synthesis protocols for fabricating Au nanoplates with small edge sizes (<200 nm) do exist.[8] Recently, some groups reported the synthesis and the NIR absorption of Au microplates through reduction of Au precursor in solution with the presence of different growth habit modifiers.[9] At present, the fabrication of Au plates with large size, well-defined morphologies, and high-yield is still a great challenge.

In applied science, it is known that the shape-dependent optical properties of Au and Ag nanostructures, and especially the high absorption efficiency in the NIR region, are promising in biomedical diagnostics, biosensors, and heat absorption in special equipment.[7,9c,10] However, studies on the Au nanoparticles have also shown the size and shape effect on the thermodynamic stability. For spherical Au particles, the melting temperatures decrease sharply from ∼1100 K for 5 nm to 600 K for 2 nm, while the melting temperature increases slowly when the size is larger than 10 nm.[11] Actually, the melting point of Au nanostructure (such as Au nanorods) measured experimentally decreases much more than the prediction, especially for the large sized particles, as reported by El-Sayed et al.[12] Therefore, it is also important to check the thermal stability of Au nanostructures for their potential applications at elevated temperatures.

In this paper, we present a simple method for fabricating Au microplates in high quantities and with regular shapes via thermal reduction (80∼150 °C) of $HAuCl_4$ in ethylene glycol at the presence of poly(vinylpyrrolidone) (PVP). The method is more or less similar to the polyol process as described by Sun et al. and Bonet et al., when they synthesized Ag nanowires and monodisperse Pt-group metal nanoparticles, respectively.[3g,13] The obtained Au microplates with edge length up to 50 μm are single crystals with (111) planes as the basal surfaces. Optical properties of such anisotropic Au nanostructure show distinct dipole and quadrupole absorption bands in the NIR region. Thermal stability studies on the sample indicate that Au microplates are disintegrated into pieces when temperature is

* Corresponding author. E-mail address: cxkan@nju.edu.cn, Tel: +86−25−83595082, Fax: +86-25-83595535.
† Nanjing University.
‡ Chinese Academy of Sciences.

10.1021/jp054800d CCC: $33.50
Published on Web 02/21/2006

higher than 450 °C. Presented below are details of the investigation.

2. Experimental Section

2.1 Preparation of Au Microplates. In a typical synthesis, 1 mL of $HAuCl_4$ (0.2 M) solution was added to 6 mL ethylene glycol that was stirred slowly at 150 °C in a round-bottom flask (equipped with thermometer). Then 3 mL ethylene glycol solution of poly(vinylpyrrolidone) (PVP 222 mg/mL, Mw = 40 000) was injected dropwise (the molar ratio of PVP/Au is 30). The reaction mixture was continuously stirred at 150 °C and sampled at different times. After ~10 min, shining products appeared in the mixture and increased progressively with the reaction time. The growth of microplates was monitored under an optical microscope by sampling a small drop of the reaction mixture on glass slides. Because the high boiling temperature (198 °C) of ethylene glycol and gelation property of PVP will bring negative influence on the following characterizations, the reaction mixtures sampled at different times were diluted with acetone (3× by volume) and centrifuged at 2500 rpm for 20 min, and the solvent containing residual reactants was decanted. The products were then rinsed with deionized water and centrifuged repeatedly to remove the possible contamination.

2.2 Characterization. Field-emission scanning electron microscopic (FE-SEM) measurements were carried out with a microscope (ESEM, Sirion200, FEG) operated at 20 kV. The X-ray diffraction (XRD) pattern was conducted on a diffractometer (Ultima-III, Rigaku) with Cu Kα radiation. Transmission electron microscopy (TEM) images and selected-area electron diffraction (SAED) studies for the products prepared on carbon-coated copper grids were taken with JEM-200CX apparatus using an acceleration voltage of 200 kV. High-resolution transmission electron microscopy (HRTEM) studies were performed with a TECNAI G^2 instrument (operated at 200 kV). Micrographs were digitalized for image processing using a high-resolution CCD camera. Optical absorption spectra for the samples were recorded on a Carry-5E (UV−vis−NIR) spectrophotometer. For optical absorption measurement, the products were prepared, respectively, by depositing on glass substrates and by dispersing in ethylene glycol solution (Au microplates deposit quickly when they were dispersed in water). To study the thermal stability of the Au microplates, the as-prepared Au microplates deposited on quartz glass substrates and carbon-coated copper meshes were treated with different heating process under ambient atmosphere. The in situ observations on the continual changes of Au microplates upon heating were further performed on a heating stage of JEM-200CX equipment with vacuum of $\sim 10^{-7}$ Torr. For heating, the copper meshes holder was sandwiched by two heaters of molybdenum meshes.

3. Results

3.1 Structural Characterizations. Figures 1A−C show the representative FE-SEM images for Au microplates obtained at different reaction times. The flat feature of microplates is induced from their low and uniform contrast. Typically, some microplates are found to overlay the holes of the supporting substrate, yielding a different contrast of one microplate, as indicated by arrows in Figure 1A. This observation also clearly reveals the flat feature, but not polyhedral or pyramid morphology of the Au nanostructures. Interestingly, Au microplates exhibit a morphological transformation with increasing reaction time. Over 75% of the total microplates obtained at 20 min are hexagonal (see Figure 1A). The microplates sampled at 40 min

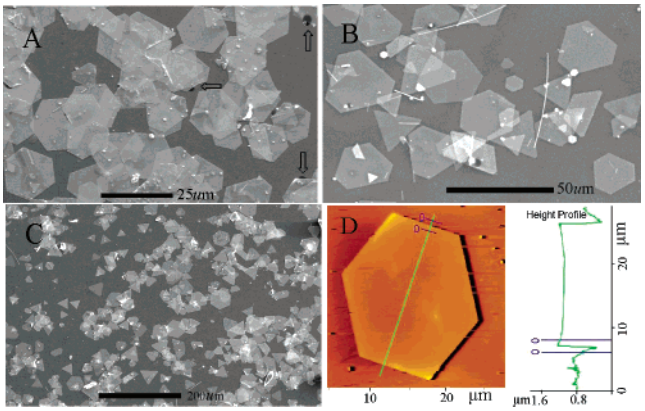

Figure 1. FE-SEM images of Au microplates sampled at different reaction time: (A) 20 min, (B) 40 min, and (C) 60 min; (D) AFM image and height profile of one Au microplate.

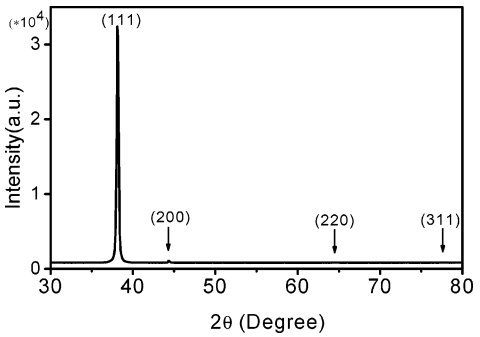

Figure 2. XRD pattern of the obtained Au microplates deposited on a glass substrate.

are a mixture of hexagonal-truncated triangular-triangular shapes, together with a few nanowires. And the final product at 60 min is dominated by nanostructures of thermodynamically stable triangular shape with sharp corners and snips (see Figure 1C). The hexagonal Au microplates obtained at 20 min are comparatively uniform with average edge size of ~10 μm. The triangular plates in the final product have a size-distribution of ~27 ±10 μm and snips less than 15%. Atomic force microscopy (AFM) was also used to define the shapes and size of the Au microplates. The line analysis on AFM images shows that the Au microplates are of around 70 nm in average thickness, as shown in Figure 1D for one hexagonal microplate.

Figure 2 presents an XRD pattern of the final products after centrifugation. It can be seen that the diffraction peak at ~38.2° assigned to the (111) lattice plane of face-centered-cubic (fcc) Au crystal shows the overwhelming intensity in the pattern, and other diffraction peaks possibly originated from a small amount of other Au nanostructures are very weak. This result implies that the basal plane, i.e., the top crystal plane of the microplates, should be the (111) plane. For the plate-like fcc metal particles, this structural configuration has been found to be quite common. It is highly possible that this plane possesses the lowest surface tension.

Figure 3 shows TEM images and the corresponding SAED patterns of Au products obtained at 5 min (Figures 3A,B) and 40 min (Figures 3C,D). In the former case, the formed Au platelet with ~100 nm in edge length is accompanied by many small nanoparticles. The SAED pattern corresponds to Au crystal viewed along a ⟨111⟩ direction, indicating the single-crystalline structure of this hexagonal platelet. Besides three sets of regular Bragg diffractions spots of {220} {422} and {440} type (marked by circles), the SEAD is dominated by kinematically fractional (forbidden) {422} spots, as labeled in

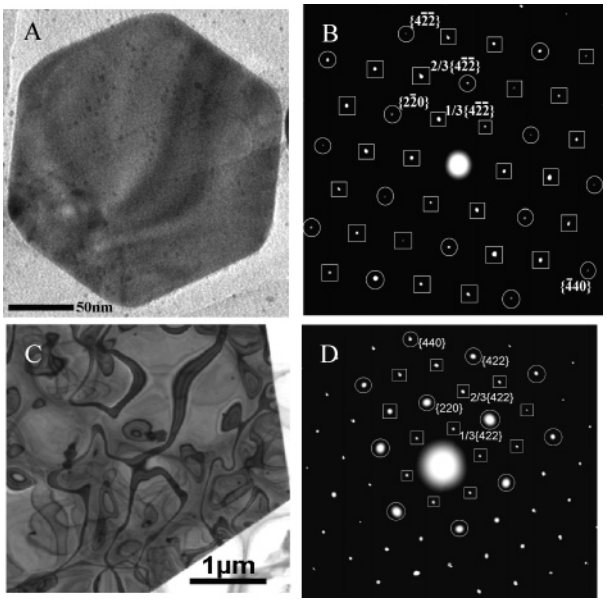

Figure 3. TEM images and the corresponding SAED patterns of the Au platelets obtained at 5 min (A−B) and 40 min (C−D). The SEAD patterns were taken from the platelets against one of two basal facets. The regular spots indexed to the {220}, {422}, and {440} reflections are marked by circles, other spots assigned to the fractional {422} reflections are marked by boxes.

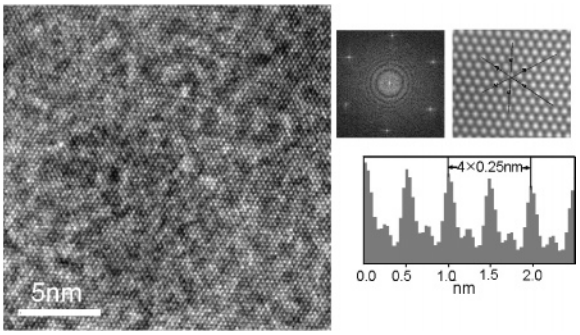

Figure 4. HRTEM image and analyses of the Au microplate.

boxes. In the latter case, most of the Au plates are more than 10 *u*m in edge size. Moreover, the observed microplates are decorated by many bending contours, diffraction effects resulting from slight bending of the thin microplates, as clearly displayed by Figure 3C for one part of an Au microplate. The SAED patterns taken from various regions of this microplate are nearly identical, as shown in Figure 3D, indicating the same spot configuration as presented in Figure 3B. However, the intensity of diffraction spots, especially the set of {220} type, is stronger than that of Figure 3B. Usually, there are two possible reasons for the appearance of the fractional {422} reflections. (1) The effect of the double diffraction of electrons. Because the diffraction of electron is much stronger than that of the presumption in kinematics, the diffraction electrons beam can be used as an incident electrons beam, diffracting again in crystal. (2) The existence of unique (111) stacking fault parallel to the (111) surface. In many related works, the latter one is often proposed to explain the forbidden {422} diffractions in [111] SAED pattern. The change in the intensity with various samples is probably due to the different (111) stacking sequence and slight difference in thickness of the plates.

Further studies on the fine microstructure of the Au microplates were performed by means of HRTEM. Figure 4 shows the HRTEM image of the [111] orientated Au microplate, in

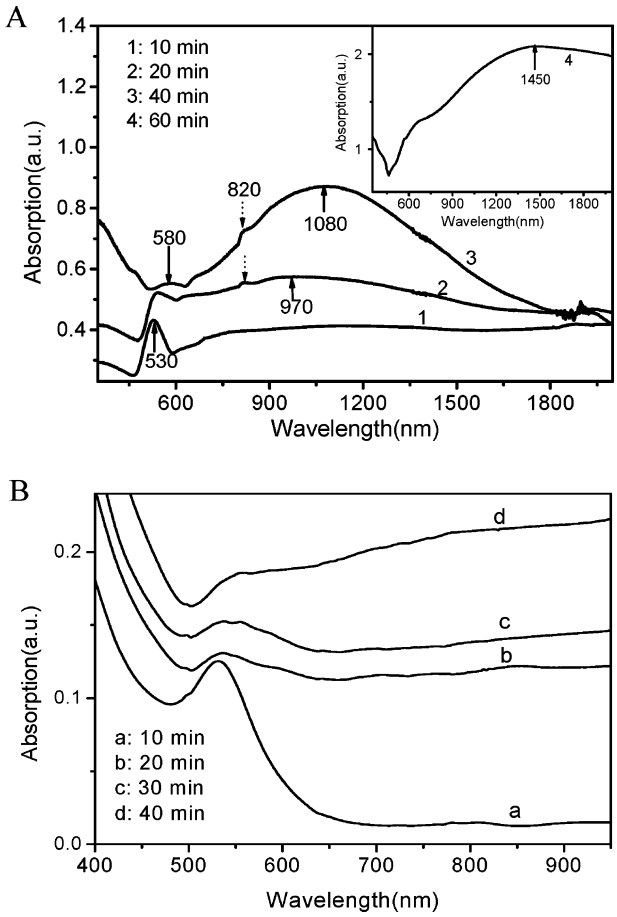

Figure 5. Optical spectra of Au products obtained at different reaction time during the sample preparation process. (A) Dispersed in ethylene glycol and (B) deposited on glass substrate.

which the corresponding fast Fourier transform (FFT), inverse FFT, and histograms of fringe spacing collected from the inverse FFT are provided. The HRTEM investigations indicated that the well-resolved crystal lattices fringes are continuous even for the part with bending contour. The most frequently observed fringe spacing of ∼0.25 nm measured from the inverse FFT (and HRTEM images) deviates distinctly from the {111} lattice plane spacing (0.235 nm) of Au crystal. Instead, it agrees fairly well with three times the {422} lattice (or 3×{422} superlattice) spacing (0.249 nm) of Au crystal. This observation is consistent with the SAED analyses and is expected to appear in thin films or platelets with {111} surfaces in the perpendicular direction. From HRTEM observations, it is also demonstrated that these 3×{422} superlattice fringes build a perfect lattice across the entire microplates, including the regions with thickness gradient.

3.2 Optical Properties. The highly structural anisotropy of the Au microplates and the orientation of plates to the incident beam should substantially modify the resulting spectra, since the polarized moment is very anisotropic.[2,4e] For the platelets, dipole and higher surface plasmon modes (such as a quadrupole plasmon resonance) for both in-plane and out-of-plane polarizations will appear. For transverse-magnetic polarization, where the incident magnetic field is in the plane, plasmons cannot be excited. Thus, in the optical spectra measurement, the sample preparation methods (deposited on flat glass slide or dispersed in solution) will influence the results. Figure 5 compares the optical spectra of Au products dispersed in ethylene glycol and deposited on glass substrate. For the Au microplates dispersed in solution, two main absorption maxima are generally observed in their optical spectra, as indicated by solid arrows in Figure

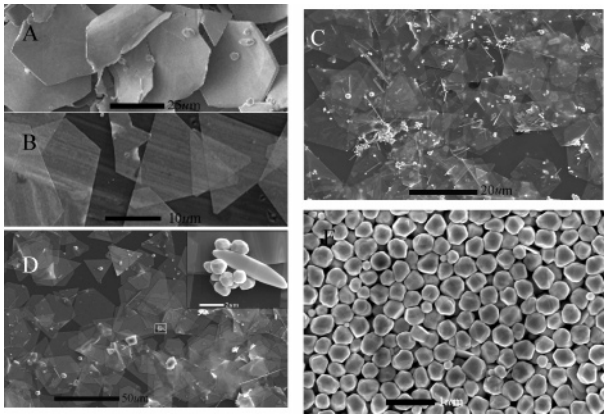

Figure 6. FE-SEM images of Au microplates synthesized at 150 °C with the PVP/Au ratios of 7.5 (A), 20 (B) and 45 (C), Au nanostructures synthesized at 80 °C with ethylene glycol and deionized water as solvents are respectively shown in (D) and (E). The sample for (B) was deposited on one scraped substrate. Inserted in (D) is a magnification image for the polyhedral Au nanostructures of box part.

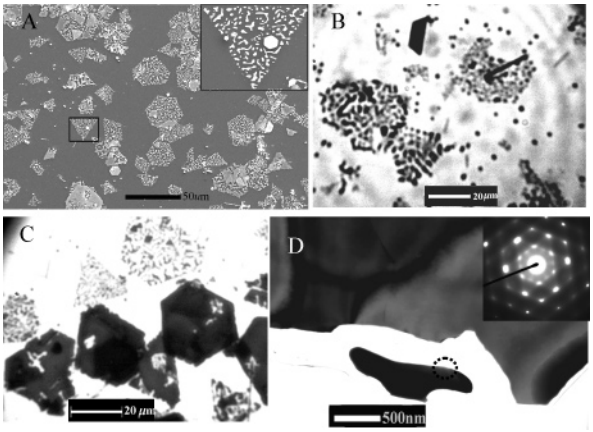

Figure 7. (A) FE-SEM and (B) optical microscope images of Au microplates after annealing for 2 h, respectively, at 500 °C and 700 °C. (C) Optical microscope image of Au microplates (mixture of thin and thick ones) after heating at 550 °C for 1 h. (D) One of typical in situ TEM image and SAED for Au microplates at 500 °C for 10 min, reflecting the process of islands formation on the plate just is beginning.

5A. The first peak appeared at ∼530 nm (see curve 1) is assigned to the dipole resonance associated with small spherical Au nanoparticles. This SPR peak shifts to about 540 and 580 nm for the samples obtained at 20 and 40 min, indicating increases in the spherical particles sizes. The second distinct plasmon absorption band centered at ∼960 nm (curve 2) is broad, coupling with another band that appears at 820 nm (as indicated by dot arrows). These two bands should correspond to the resonances over much larger distances of flat shapes, in which the oscillation of free electrons was strongly restricted in the planar structure. With increase of reaction time, the broad absorption band shifts to ∼1080 (curve 3) and 1450 nm (curve 4). Based on the prediction of discrete dipole approximation,[14] the reddest broad band of each curve and the band at 820 nm should be assigned, respectively, to the in-plane dipole resonance and in-plane quadrupole mode of the Au microplates. Here, it is notable that quadrupole resonance of Au nanostructures is rarely observed in related literatures possibly due to inhomogeneity and impurities in sample. A recent contribution from Mirkin et al. has produced a similar quadrupole resonance at ∼814 nm.[15] For the sample of 60 min, the SPR of spherical particles (if any) was overlapped with the broad in-plane dipole resonance (see inset) and the in-plane quadrupole resonance was "quenched", similar to the Ag particles with large aspect ratio.[4e] However, for the Au products dispersed on glass slides, only one obvious SPR peak at 530∼550 nm of spherical Au nanoparticles was observed with ever-decreasing intensity with time, accompanied by absorption in the NIR region (see curves a−d of Figure 5B).

3.3 Growth Conditions for Au Microplates. For better understanding the growth of Au microplates, a set of experiments have been further carried out to establish the role of PVP, reaction temperature, and solvent on the growth of microplates. At a reaction temperature of 150 °C, it is found that the molar ratios of PVP (repeating units)/$HAuCl_4$ between 15 and 30 are favorable for the growth Au microplates. When the ratio is reduced, the thickness of the formed Au microplates increases obviously. Figure 6A and 6B present the FE-SEM images of Au microplates synthesized with PVP/Au ratios of 7.5 and 20, respectively. The contrasts of the overlapped microplates, and especially the visible scrape of substrate underlying the microplates in Figure 6B, clearly demonstrate that the microplates are thinner than the microplates in Figure 6A (the difference in thickness is also confirmed by AFM measurements). In the absence of PVP, the time for completion of reaction is more than 3h and the final product is mainly composed of aggregated polyhedral Au particles coexisting with a small fraction of thick plates. On the contrary, the reaction will be accelerated upon an increase of PVP concentration. However, in addition to the Au microplates, large numbers of small spherical, rod-like and polyhedral Au nanoparticles are formed in the sample (see Figure 6C), revealing that high concentration of PVP is also unfavorable for the growth of Au microplates. Through adjusting the experiment temperature, we found that Au microplates could be actually obtained at a low temperature (<100 °C) with a fixed PVP/Au ratio of 20 (see Figure 6D). In this case, some polyhedral Au nanoparticles are also found, as inserted in Figure 6D. When deionized water instead of ethylene glycol was used as the solvent (the PVP/Au ratio was 30), the reaction proceeded slowly at 80 °C and the final product was dominated by polyhedral Au particles of ∼400 nm in size, as shown in Figure 6E. These results undoubtedly suggest that, in addition to its function of generating a stable colloid, PVP not only has a reduction effect on metal ions, as previously reported,[16] but also plays, together with ethylene glycol, a shape-directing role in the formation of Au microplates.

3.4 Morphology Changes of Au Microplates upon Heating. The thermal stability of the formed Au microplates was investigated by treating the microplates loaded on quartz substrate with different heating process. When the temperature is lower than 400 °C, there is no obvious change on the Au microplates by SEM observation. However, when the sample was annealed at a temperature >450 °C, Au microplates would be disintegrated into many islands (or particles), as typically presented in Figure 7A for Au microplates annealed at 500 °C for 2 h. The most interesting phenomenon is that the fragmented particles still keep the original outlines of the plates, as illustrated by the inset for the boxed one. The original shapes will be destroyed when the Au microplates were annealed at 700 °C, at which the formed Au nanoparticles are nearly spherical and dispersed randomly (see Figure 7B). In case of thick Au microplates, the cracking process on them just begins at ∼550 °C, while the thin ones have been completely disintegrated into pieces, as shown in Figure 7C.

From the in situ TEM observations on the continual morphology changes of Au microplates upon heating, we found that the degeneratiaon of Au microplates starts primarily at the edge parts, as typically illustrated by Figure 7D for the sample heated

at ~500 °C for 10 min, in which the trace of edge shrinkage can be clearly seen. The SAED pattern indicates that the fragmented Au particle has the same crystal structure as that of the as-prepared Au microplates. According to the temperature applied, the heat effect should be stronger, but this was in vacuum where metal vapor-phase species near the plate surface get more easily removed and where temperature measurement may be more erroneous (the heating temperature, at which Au microplates begin to break, measured in situ TEM is higher than that in ambient atmosphere).

4. Discussion

4.1 Growth Mechanism for Au Microplates. The exact growth process of the large-sized Au plates has yet to be established, although some groups have presented the growth mechanism for anisotropic nanostructures synthesized by solution phase methods. The standard explanation for the formation of microplates usually involves the role of preformed "seed" and the appropriate capping reagents that used to control the growth rate of various facets of the preformed seeds.

In the literature, polymers were often used to prepare metal nanoparticles, in which the polar groups interact directly with the particles surface and strongly influence particles shape.[9] It is known that PVP has affinity toward many chemicals due to its polyvinyl skeleton with strong polar pyrrole rings.[16] Recently, ethylene glycol was often used (as both solvent and reducing agent) to prepare metal nanoparticles thanks to its polar hydroxyl groups, which are capable of complexing with surfaces of metal nanoparticles through direct interaction.[17]

On the other hand, the growth rates of crystal are often controlled (kinetically rather than thermodynamically) by the sticking probability on a given face.[18] Since the (111) face of fcc metal has the lowest sticking probability being of lowest surface energy compared to other faces ($\gamma_{(110)} > \gamma_{(100)} > \gamma_{(111)}$), the fcc metal confers its tendency to nucleate and grow into nanoparticles with their surfaces bounded by (111) facets, particularly in the process of chemical synthesis.

Accordingly, it is reasonable to speculate that Au nuclei formed in the initial stage are kinetic structures with lowest-energy (111) surfaces. Then at a favorite PVP/Au molar ratio, the polar groups, such as pyrrole rings of PVP and hydroxyl groups of ethylene glycol molecules, adsorb preferentially on the sites of the {111} planes of Au nuclei and interact with the {111} planes, which also obviously slows (or prevents) the growth on the (111) plane and promotes a highly anisotropic crystal growth, such as along ⟨110⟩ orientation, extending into large microplates with basal {111} planes. However, less or excessive PVP coverage on the surfaces of Au nanoparticles would induce a simultaneous growth for different crystal faces to some extend (or even growth limitation) apart from the anisotropic growth within the (111) plane, leading to the formation of multishaped of Au nanostructures.

Another accepted opinion suggested that PVP merely acts as a stabilizer and that the presence of planar defects (such as stacking faults and twins) on the {111} planes of the seeds induces fast growth of a certain plane(s), leading to the formation of the microplates, although the exact structure of these seeds has yet to be established.[4h,19]

4.2 Thermal Stability of Au Microplates. As a consequence of the improved surface energy (or others), the melting point of Au nanoparticles is depressed from that of the bulk material. However, in our experiment the Au microplates begin to melt at 450~500 °C, far below the melting point of the size-dependent prediction.[11a,20]

In the studies of melting behavior of Au nanostructures upon thermal treatment, it is revealed the melting phenomenon usually takes place only on the (110) facets or edges at low temperatures, while the (111) surface remains crystalline up to and even above the melting point.[11b,21] For example, the surface melting could occur at ~500 °C for Au nanoparticles with ⟨110⟩ orientation, as reported by Hoss et al. and Wojtczak et al.[22] Therefore, in our case, the surface melting areas should be impossible to observe in Au microplate surfaces, where only (111) planes are present. However, the disintegration of the Au microplates occurs at ~450 °C. More importantly, the in situ TEM observation indicates that the process of Au island formation on Au microplates begins at the edge part, as shown in Figure 7D. These experimental results imply that the Au microplates grow in ⟨110⟩ directions, i.e., the edges should be Au (110) facets, although the statement was not directly proved in experiment.

Although the SAED results indicate the single-crystalline nature of the formed Au microplates, some irregularities, such as terrace, vacancy, and atomic step, would inevitably exist on the large surface. Being affected from surface tension and irregular atom arrangement, the Au microplates have high surface energy, which brings a reduction trend of surface. When the heat impact is strong enough, Au microplates will break up into smaller but thicker islands, leading to a distinct reduction of the surface energy.

Based on the above discussions, we can also see that the kinetically controlled morphologies (such as platelet) do not mean they are thermodynamically stable structures.

5. Conclusions

In summary, this paper provides a simple solution-phase method for synthesizing Au microplates with regular shape and large edge size up to ~50 μm. The obtained Au microplates are single crystals with (111) plane as basal surfaces. The stronger adsorption of polar groups of reactants on the (111) plane of Au nuclei accounted for the anisotropic growth of microplates. In view of the striking NIR absorption of Au metal, the planar Au microplates are expected to have potentials in many fields, and one exciting application is to turn this nanostructure into biomedical tool for diagnosing tumor cells. Investigations on the thermal stability of Au microplates indicate that they are not thermodynamically stable, and that the melting and cracking starts from the edge parts that should be bounded by Au (110) surface. Thus, the study on the thermal stability of Au microplates is also valuable for Au nanostructures applied at elevated or a given high temperature.

Acknowledgment. This work was financially supported from the National Natural Science Foundation of China (Grant No.90206033), FANEDD (No. 200421), China Postdoctoral Science Foundation, and Jiangsu Planned Projects for Postdoctoral Research Funds. C.K. is indebted to Prof. Jianmin Hong and Dr. Zhaosheng Li for their great help with the in situ TEM observation XRD measurements of samples upon heating. Discussions with Prof. Herbert Hofmeister of Max Planck Institute Microstructure Physics (Germany) on the SAED and anisotropic growth are also gratefully acknowledged.

References and Notes

(1) (a) Kreibig, U.; Vollmer, M. In *Optical Properties of Metal Clusters*; Gonser, U., Osgood, R. M., Panish, M. B., Jr., Sakaki, H., Eds.; Springer: New York, 1995; Ch. 2. (b) Bohren, C. F.; Huffman, D. R. In *Absorption and Scattering of Light by Small Particles*; John Wiley & Sons: New York, 1998; Ch. 12.

(2) (a) Kottmann, J. P.; Martin, O. J. F.; Smith, D. R.; Schultz, S. *Phys. Rev. B* **2001**, *64*, 235402. (b) Kottmann, J. P.; Martin, O. J. F.; Smith, D. R.; Schultz, S. *Chem. Phys. Lett.* **2001**, *341*, 1.

(3) (a) Yu, Y. Y.; Chang, S. S.; Lee, C. L.; Wang, C. R. C. *J. Phys. Chem. B* **1997**, *101*, 6661. (b) Link, S.; Mohamed, M. B.; El-Sayed, M. A. *J. Phys. Chem. B* **1999**, *103*, 3073. (c) van der Zande Bianca, M. I.; Marcel, R. B.; Lambertus, G. J. F.; Christian, S. *Langmuir* **2000**, *16*, 451. (d) Jana, N. R.; Gearheart, L.; Murphy, C. J. *J. Phys. Chem. B* **2001**, *105*, 4065. (e) Busbee, B. D.; Obare, S. O.; Murphy, C. J. *Adv. Mater.* **2003**, *15*, 414. (f) Sloan, J.; Wright, D. M.; Woo, H. G.; Bailey, S.; Brown, G.; York, A. P. E.; Coleman, K. S.; Hutchison, J. L.; Green, M. L. H. *Chem. Commun.* **1999**, 699. (g) Sun, Y. G.; Xia, Y. N. *Adv. Mater.* **2002**, *14*, 833.

(4) (a) Jin, R. C.; Cao, Y. W.; Mirkin, C. A.; Kelly, K. L.; Schatz, G. C.; Zheng, J. G. *Science* **2001**, *294*, 1901. (b) Chen, S. H.; Carroll, D. L. *Nano Lett.* **2002**, *2*, 1003. (c) Hao, E.; Kelly, K. L.; Hupp, J. T.; Schatz, G. C. *J. Am. Chem. Soc.* **2002**, *124*, 15182. (d) Sun, Y. G.; Mayers, B.; Xia, Y. N. *Nano Lett.* **2003**, *3*, 675. (e) Kelly, K. L.; Coronado, E.; Zhao, L. L.; Schatz, G. C. *J. Phys. Chem. B* **2003**, *107*, 668. (f) Zhao, Q. T.; Hou, L. S.; Zhao, C. J.; Gu, S. P.; Huang, R. A.; Ren, S. H. *Laser Phys. Lett.* **2004**, *1*, 115. (g) Okada, N.; Hamanaka, Y.; Nakamura, A.; Pastoriza-Santos, I.; Liz-Marza, L. M. *J. Phys. Chem. B* **2004**, *108*, 8751. (h) Métraux, G. S.; Mirkin, C. A. *Adv. Mater.* **2005**, *17*, 412.

(5) (a) Yu, D. B.; Yam, V. W. *J. Am. Chem. Soc.* **2004**, *126*, 13200. (b) Chen, S. H.; Wang, Z. L.; Ballato, J.; Foulger, S. H.; Carroll, D. L. *J. Am. Chem. Soc.* **2003**, *125*, 16186. (c) Sun, Y. G.; Xia, Y. N. *Science* **2002**, *298*, 2176.

(6) Chen, S. H.; Carroll, D. L. *J. Phys. Chem. B* **2004**, *108*, 5500.

(7) (a) Simpson, C. R.; Kohl, M.; Essenpreis, M.; Cope, M. *Phys. Med. Biol.* **1998**, *43*, 2465. (b) Haes, A. J.; Van Duyne, R. P. *J. Am. Chem. Soc.* **2002**, *124*, 10596. (c) Chen, J. Y.; Saeki, F.; Wiley, B. J.; Cang, H.; Cobb, M. J.; Li, Z. Y.; Au, L.; Zhang, H.; Kimmey, M. B.; Li, X. D.; Xia, Y. N. *Nano Lett.* **2005**, *5*, 473.

(8) (a) Malikova, N.; Pastoriza-Santos, I.; Schierhorn, M.; Kotov, N. A.; Liz-Marzan, L. M. *Langmuir* **2002**, *18*, 3694. (b) Sau, T. K.; Murphy, C. J. *J. Am. Chem. Soc.* **2004**, *126*, 8648.

(9) (a) Shao, Y.; Jin, Y. D.; Dong, S. J. *Chem. Commun.* **2004**, (9), 1104. (b) Wang, L. Y.; Chen, X.; Zhan, J.; Chai, Y. C.; Yang, C. J.; Xu, L. M.; Zhuang, W. C.; Jing, B. *J. Phys. Chem. B* **2005**, *109*, 3189. (c) Shankar, S. S.; Rai, A.; Ahmad, A.; Sastry, M. *Chem. Mater.* **2005**, *17*, 566. (d) Sun, X. P.; Dong, S. J.; Wang, E. K. *Langmuir* **2005**, *21*, 4710.

(10) (a) Bauer, L. A.; Birenbaum, N. S.; Meyer, G. J. *J. Mater. Chem.* **2004**, *14*, 517. (b) Haes, A. J.; Zou, S. L.; Schatz, G. C.; Van Duyne, R. P. *J. Phys. Chem. B* **2004**, *108*, 109.

(11) (a) Buffat, P.; Borel, J. P. *Phys. Rev. A* **1996**, *13*, 2287. (b) Liu, H. B.; Ascencio, J. A.; Perez-Alvarez, M.; Yacaman, M. J. *Surf. Sci.* **2001**, *491*, 288.

(12) Mohamed, M. B.; Wang, Z. L.; El-Sayed, M. A. *J. Phys. Chem. A* **1999**, *103*, 10255.

(13) (a) Sun, Y. G.; Yin, Y. D.; Mayers, B. T.; Herricks, T.; Xia, Y. N. *Chem. Mater.* **2002**, *14*, 4736. (b) Bonet, F.; Delmas, V.; Grugeon, S.; Urbina, R. H.; Silvert, P. Y.; Tekaia-Elhsissen, K. *Nanostruct. Mater.* **1999**, *11*, 1277.

(14) Draine, B. T.; Flatau, P. J. *J. Opt. Soc. Am. A* **1994**, *11*, 1491.

(15) Millstone, J. E.; Park, S.; Shuford, K. L.; Qin, L. D.; Schatz, G. C.; Mirkin, C. A. *J. Am. Chem. Soc.* **2005**, *127*, 5312.

(16) Kan, C. X.; Cai, W. P.; Li, C. C.; Zhang, L. D. *J. Mater. Res.* **2005**, *20*, 320.

(17) Kamat, P. V. *J. Phys. Chem. B* **2002**, *106*, 7729.

(18) (a) Marks, L D. *Rep. Prog. Phys.* **1994**, *57*, 603649. (b) Nam, H. S.; Hwang, N. M.; Yu, B. D.; Yoon, J. K. *Phys. Rev. Lett.* **2002**, *89*, 275502.

(19) (a) Germain, V.; Li, J.; Ingert, D.; Wang, Z. L.; Pileni, M. P. *J. Phys. Chem. B* **2003**, *107*, 8717. (b) Wiley, B.; Sun, Y. G.; Chen, J. Y.; Cang, H.; Li, Z. Y.; Li, X. D.; Xia, Y. N. *MRS Bull.* **2005**, *30*, 356.

(20) (a) Gibbs, D.; Ocko, B. M.; Zehner, D. M.; Mochrie, S. G. J. *Phys. Rev. B* **1990**, *42*, 7330. (b) Dick, K.; Dhanasekaran, T.; Zhang, Z. Y.; Meisel, D. *J. Am. Chem. Soc.* **2002**, *124*, 2312.

(21) (a) Ercolessi, F.; Andreoni, W.; Tosatti, E. *Phys. Rev. Lett.* **1991**, *66*, 911. (b) Wang, Y. T.; Teitel, S.; Dellago, C. *Chem. Phys. Lett.* **2004**, *394*, 257.

(22) (a) Hoss, A.; Nold, M.; von Blanckenhagen, P.; Meyer, O. *Phys. Rev. B* **1992**, *45*, 8714. (b) Wojtczak, L.; Rutkowski, J. H. *Prog. Surf. Sci.* **1998**, *59*, 79.